

Impedance analysis and conduction mechanism of Ba doped $\text{Mn}_{1.75}\text{Ni}_{0.7}\text{Co}_{0.5-x}\text{Cu}_{0.05}\text{O}_4$ NTC thermistors

Muhammad Asif Rafiq¹ · Muhammad Tayyab Khan¹ · Qaisar Khushi Muhammad¹ · Moaz Waqar¹ · Furqan Ahmed¹

Received: 29 December 2016 / Accepted: 14 August 2017 / Published online: 21 August 2017
© Springer-Verlag GmbH Germany 2017

Abstract Polycrystalline $\text{Mn}_{1.75}\text{Ni}_{0.7}\text{Co}_{0.5-x}\text{Cu}_{0.05}\text{Ba}_x\text{O}_4$ ($x = 0, 0.05$ and 0.1) based negative temperature coefficient (NTC) thermistors were synthesized using conventional solid state reaction method. X-ray diffraction (XRD) analysis confirmed the presence of single phase cubic spinel structure for all the compositions and successful substitution of Ba. Scanning electron microscopy (SEM) revealed a dense microstructure along with slight increase in grain size due to Ba doping. Impedance spectroscopy (IS) studies showed that the increase in temperature caused both grain and grain boundary resistance to decrease indicating NTC behavior of the samples. The grain boundary resistance was several magnitudes greater than the resistance of grains which showed that the NTC characteristic of doped samples was mainly dependent on grain boundaries. The time constant for both grain and grain boundary decreased with temperature indicating a hopping conduction mechanism. These results can lead to design the optimum microstructure for various practical applications of NTC thermistors.

1 Introduction

Negative temperature coefficient (NTC) thermistors are mainly used for domestic and industrial applications, e.g., aerospace, automotive, circuit compensation, control applications, and temperature measurement [1]. NTC

thermistors have been recognized as the most effective electronic instruments in thermal sensor industry for the last few decades [1–3]. Transition metal oxides such as Nickel Oxide (NiO), Cobalt Oxide (CoO) and Manganese Oxide (MnO) are mainly used as NTC thermistors due to the decrease in their electrical resistance with increase in temperature [1, 4–6]. Among all these variants, Nickel Manganite (NiMn_2O_4) based compositions are well suited to be used as an NTC thermistor material in specific temperature applications since it is the family of controlled valence semi-conductors whose electrical resistance decreases exponentially with an increase in temperature. It crystallizes in the cubic spinel (AB_2O_4) structure, based upon the cubic close packing of oxygen ions in which cations stand on both tetrahedral (A) and octahedral (B) sites.

Broad studies can be found in literature on the modification of Nickel Manganite NTC thermistor which suggests that thermistor characteristics are generally tailored via doping of suitable ions or via changing the processing conditions, e.g., rate of cooling, sintering temperature, sintering time, etc. [7–9]. Resistivity of NTC thermistors can be tuned by controlling and modifying these factors [10].

The main NTC thermistor parameters are room temperature resistivity (ρ_{298}), thermistor constant (β -value) and temperature coefficient of resistance (α). The electrical parameters, β -value and ' α ' could be derived from the resistance temperature characteristics. These key parameters define the conditions under which a thermistor material may be utilized. ' q ' is the activation energy for the hopping process which can be derived from the resistance (R) and thermodynamic temperature (T) relationship of NTC thermistor represented as follows;

$$R = A \exp\left(\frac{q}{kT}\right), \quad (1)$$

✉ Muhammad Asif Rafiq
asifrafiq@uet.edu.pk

¹ Department of Metallurgical and Materials Engineering,
University of Engineering and Technology, Lahore,
Punjab 54890, Pakistan

where A is constant associated to the device dimensions and resistivity (ρ) whereas ' k ' is Boltzmann's constant.

β -value is the ratio, i.e., ' q/k ' and usually calculated via following relation;

$$\beta_{298/358} = \left[T_{298} T_{358} \ln \left(\frac{R_{298}}{R_{358}} \right) \right] / (T_{358} - T_{298}), \quad (2)$$

where R_{298} and R_{358} are the resistance values at 298 K (T_{298}) and 358 K (T_{358}), respectively. Further, the temperature coefficient of resistance (α) could be defined as the rate of change of resistance (R) with thermodynamic temperature (T) to the resistance at a definite temperature and is given by following relation;

$$\alpha_{298} = \left[\frac{\left(\frac{1}{R} \right) dR}{dT} \right] = - \frac{\beta}{T^2} \quad (3)$$

It is very clear from the literature that for applications such as inrush current limiters, NTC thermistors with low resistivity and moderate sensitivity are required. [3, 11]. A comparison of these parameters for important NTC compositions is listed in Table 1.

In terms of fundamental research, most work has been devoted to the basic structural and electrical characterization of NTC thermistors based on doping of NiMn₂O₄ ceramics. Co and Cu co-doped based NTC thermistors have already been known as an outstanding choice due to their better electrical properties and higher reproducibility [1, 6]. In previous studies, Co co-substitution has been done in NiMn₂O₄ while keeping the ratio of Ni to Mn (Ni:Mn) constant [13, 16, 17]. It is found that doping with transition metal ions, e.g., Zn, Fe, Co, Cr [5, 9, 18–21] and non-transition metal ions such as Mg, Sr, Al resulted in improved electrical properties [4, 6, 15, 22]. A comprehensive report on the effect of substitution of Co in NiMn₂O₄ NTC thermistors by varying Ba concentration while keeping the Ni: Mn ratio constant is still scarce. A variation of dopant concentration is expected to cause substantial changes on the electrical properties of samples because of the relatively bigger size of Ba ($r = 1.35 \text{ \AA}$) as compared to Co ($r = 0.75 \text{ \AA}$) [23].

AC impedance spectroscopy is known as a novel technique which is widely used to characterize the electrical behavior of ceramics [24–26]. The resistive and dielectric

properties of microstructural components, i.e., grains and grain boundaries could be separately and quantitatively studied via this innovative technique. The complex impedance analysis is also an important tool to study the charge transport mechanism in ceramics [27, 28].

The present study is focused on the detailed analysis of impedance and the effect of temperature on grain and grain boundary resistance of Ba doped Mn_{1.75}Ni_{0.7}Co_{0.5-x}Cu_{0.05}O₄ NTC thermistor ceramics. Furthermore, the effect of Ba concentration on microstructure and crystal structure is studied via scanning electron microscope (SEM) and X-ray diffraction (XRD) analysis, respectively.

2 Experimental

The conventional mixed oxide solid state route was followed to prepare Mn_{1.75}Ni_{0.7}Co_{0.5-x}Cu_{0.05}Ba_xO₄ ceramics where $x = 0, 0.05$ and 0.1 . The stoichiometric compositions (hereafter will be Mn_{1.75}Ni_{0.7}Co_{0.5}Cu_{0.05}O₄, Mn_{1.75}Ni_{0.7}Co_{0.45}Cu_{0.05}Ba_{0.05}O₄ and Mn_{1.75}Ni_{0.7}Co_{0.4}Cu_{0.05}Ba_{0.1}O₄) were prepared from NiO (BDH 99.9%), MnO₂ (AnalaR, 99.9%), BaO (Merck 99.9%), CoO (AnalaR 99.9%) and CuO (AnalaR 99.8%). Raw materials (powders) were weighed in accordance with stoichiometric compositions and mixed via ball mill for 5 h in Teflon pots using ethanol as solvent. The obtained mixture was first dried and then calcined at 900 °C for 2 h in alumina crucibles. The calcined mixture was milled again for 3 h. Green pellets of 10 mm diameter and 1 mm thickness were prepared via uniaxial pressing. Pressed sample in the form of disks were sintered at 1200 °C for 3 h.

The microstructural analysis of sintered pellets was carried out using scanning electron microscope (SEM; Nova NanoSEM 450). Crystal structure and phase analyses were done via X-ray diffraction (XRD; JEOL JDX-99C) using Ni-filtered Cu-K α radiation. To take electrical measurements, the sintered ceramics were polished and silver paste was applied on both sides of the pellets and fired at 100 °C for 30 min. High temperature (300–500 °C) dielectric response was measured as a function of frequency ($\omega = 2\pi f$) from 100 Hz to 1 MHz using 1900 QuadTech Precision LCR meter.

Table 1 Important NTC thermistor parameters

Sr. no.	Composition	α (%/K)	$\beta_{298/358}$ (K)	ρ_{298} (Ω cm)	q (eV)	Refs.
1	Ni _{0.6} Cu _{0.4} Fe _{0.1} Mn _{1.9} O ₄	–	3208	–	0.330	[12]
2	Ni ₁ Mn ₁ Co _{0.9} Fe _{0.1} O ₄	–3.66	3377	1711	0.291	[3]
3	Ni _{0.7} Mn _{1.75} Co _{0.5} Cu _{0.05} O ₄	–3.79	3373	354	0.290	[13]
4	Ni _{0.9} Co _{0.8} Mn ₁ Fe _{0.3} O ₄	–	3103	922.7	0.288	[14]
5	Mn _{1.4} Ni _{1.2} Co _{0.35} Mg _{0.05} O ₄	–	3697	14,523	0.318	[6]
6	Mn _{0.9} Co _{1.2} Ni _{0.15} Mg _{0.09} Al _{0.36} Fe _{0.3}	–4.31	3829	3800	0.312	[15]

3 Results and discussion

X-ray diffraction (XRD) technique was utilized to identify the crystalline phases and to study the effect of Ba doping on the structural characteristics of $\text{Mn}_{1.75}\text{Ni}_{0.7}\text{Co}_{0.5-x}\text{Cu}_{0.05}\text{Ba}_x\text{O}_4$ ceramics. Figure 1 shows the XRD patterns of undoped and Ba doped $\text{Mn}_{1.75}\text{Ni}_{0.7}\text{Co}_{0.5-x}\text{Cu}_{0.05}\text{O}_4$ NTC ceramics sintered at 1200 °C for 3 h. Peaks obtained from XRD were indexed and they corresponded well to the spinel structure of $\text{Mn}_{1.75}\text{Ni}_{0.7}\text{Co}_{0.5}\text{Cu}_{0.05}\text{O}_4$ in earlier reports [4, 5, 13, 29–31]. No impurity or secondary phase was observed within the detection limit of the equipment. A straight line at (311) diffraction peak at 37.45° is shown in Fig. 1 which shows a peak shift towards lower 2θ values on the substitution of Co^{2+} by Ba^{2+} which indicates an increase in the lattice parameter. Table 2 shows the lattice parameters of $\text{Mn}_{1.75}\text{Ni}_{0.7}\text{Co}_{0.5-x}\text{Cu}_{0.05}\text{Ba}_x\text{O}_4$ determined using JADE MDI software. There was an increase in the lattice parameter 'a' as Ba^{2+} concentration increased in $\text{Mn}_{1.75}\text{Ni}_{0.7}\text{Co}_{0.5-x}\text{Cu}_{0.05}\text{Ba}_x\text{O}_4$. It can be attributed to the bigger size of Ba^{2+} (1.35 Å) as compared to Co^{2+} (0.75 Å) [22].

The XRD observation is also accompanied by the SEM micrographs of the sintered pellets as shown in Fig. 2. There was a slight increase in the grain size of samples with increase in Ba from $x = 0$ to $x = 0.05$ and the density of sample increased as well. It is well-known that a dense microstructure is favorable for good reproducibility of the electrical characteristics in NTC thermistors [5]. With further increase in Ba, there was no visible change in the grain size of sample; however, grain size distribution

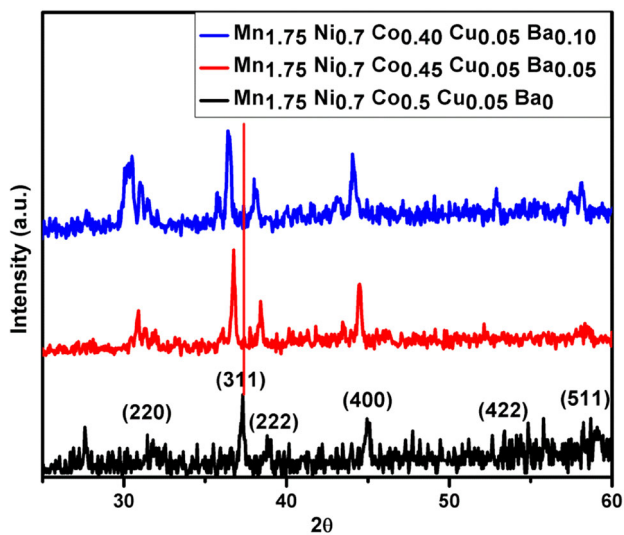


Fig. 1 XRD pattern of $\text{Mn}_{1.75}\text{Ni}_{0.7}\text{Co}_{0.5-x}\text{Cu}_{0.05}\text{Ba}_x\text{O}_4$ where ($x = 0, 0.05$ and 0.1) showing that no secondary or impurity phase was formed and peak shift towards lower 2θ values indicates the increase in lattice parameters

Table 2 Lattice parameters of $\text{Mn}_{1.75}\text{Ni}_{0.7}\text{Co}_{0.5-x}\text{Cu}_{0.05}\text{Ba}_x\text{O}_4$ where ($x = 0, 0.05$ and 0.1)

Sr. no.	Composition	Lattice parameter a (Å)
1	$\text{Mn}_{1.75}\text{Ni}_{0.7}\text{Co}_{0.5}\text{Cu}_{0.05}\text{O}_4$	7.9746
2	$\text{Mn}_{1.75}\text{Ni}_{0.7}\text{Co}_{0.45}\text{Cu}_{0.05}\text{Ba}_{0.05}\text{O}_4$	8.0711
3	$\text{Mn}_{1.75}\text{Ni}_{0.7}\text{Co}_{0.4}\text{Cu}_{0.05}\text{Ba}_{0.10}\text{O}_4$	8.1439

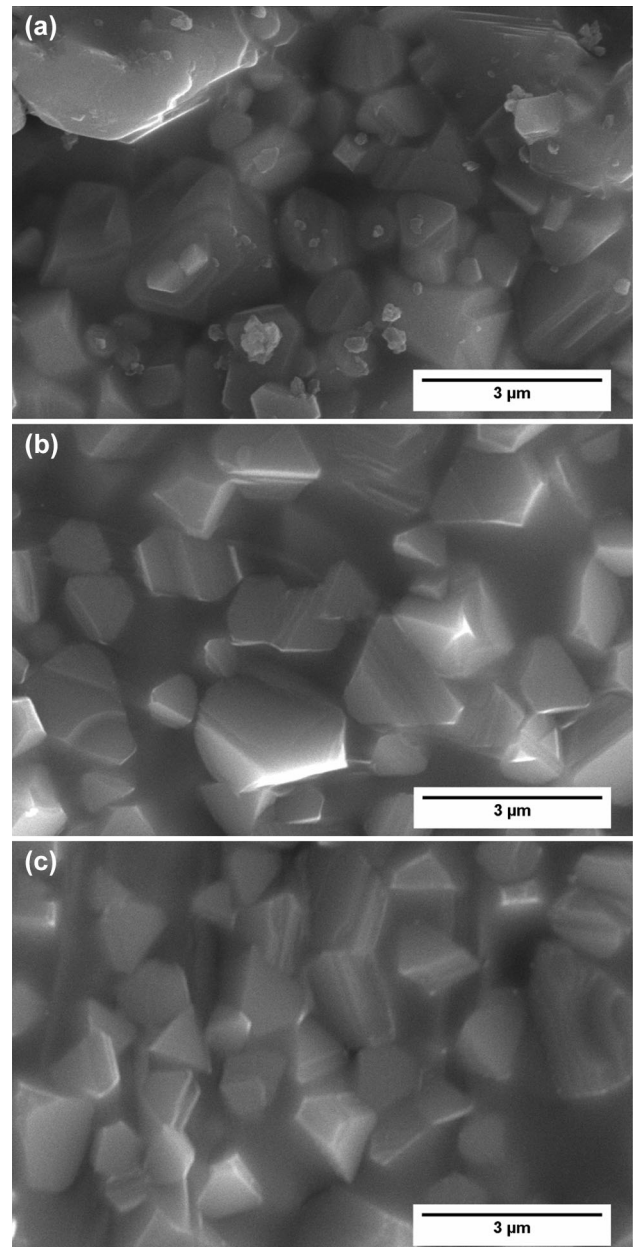


Fig. 2 SEM micrographs of $\text{Mn}_{1.75}\text{Ni}_{0.7}\text{Co}_{0.5-x}\text{Cu}_{0.05}\text{Ba}_x\text{O}_4$, **a** $x = 0$, **b** $x = 0.05$ and **c** $x = 0.1$ sintered at 1200 °C for 3 h. (A dense microstructure with enlarged grains was obtained as Ba doping was increased)

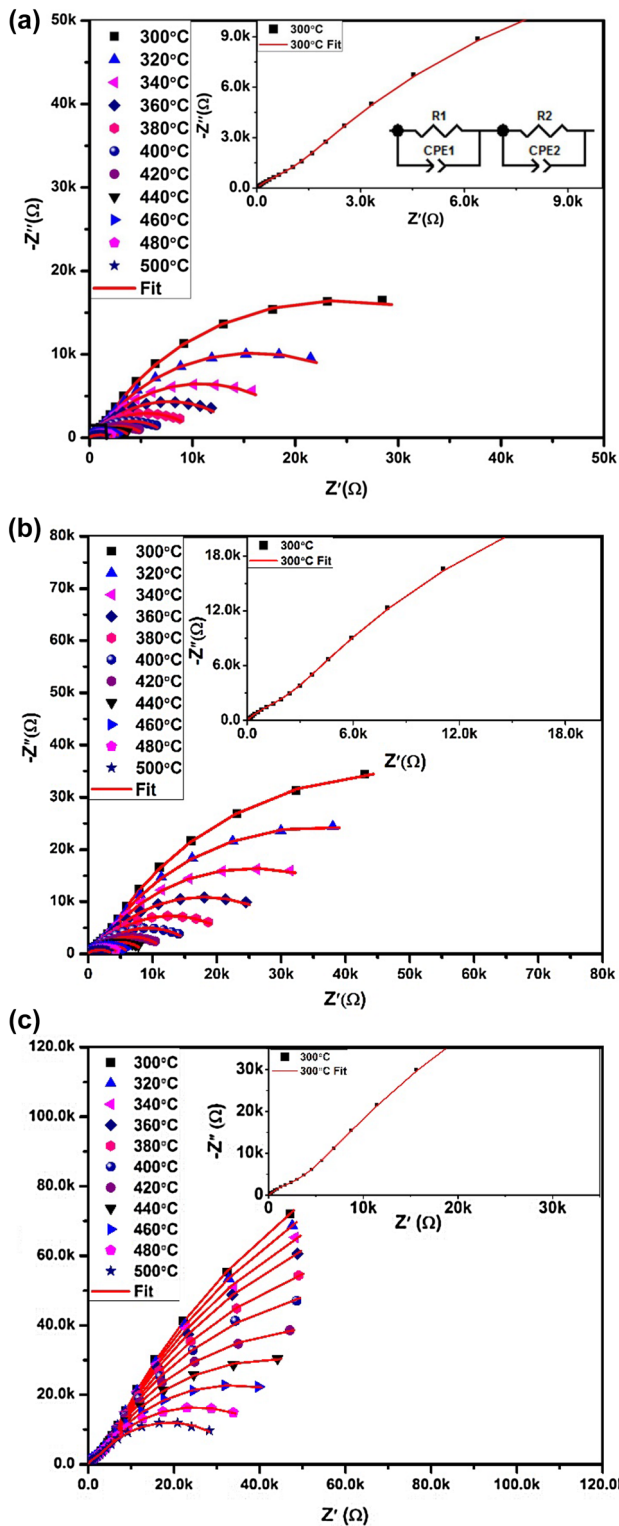


Fig. 3 Nyquist plots at 300–500 °C for $Mn_{1.75}Ni_{0.7}Co_{0.5-x}Cu_{0.05}Ba_xO_4$. **a** $x = 0$, **b** $x = 0.05$ and **c** $x = 0.1$. Fit result shown in inset shows a good agreement with experimental data

seemed more uniform at $x = 0.1$ as compared to $x = 0.05$. The results are in conformity with the previously investigated effects of Sr-doped NTC thermistors [22].

Table 3 Resistance, capacitance values determined for grain (R_1, C_1) and grain boundary (R_2, C_2) for all compositions

T (°C)	R_1 (Ω)	C_1 (nF)	N_1	R_2 (Ω)	C_2 (nF)	N_2
$Mn_{1.75}Ni_{0.7}Co_{0.5-x}Cu_{0.05}Ba_xO_4$ ($x = 0.0$)						
300	1056	1.51	0.67	27,672	13.1	0.77
320	982	1.52	0.68	18,683	13.2	0.75
340	907	1.53	0.69	12,806	13.5	0.72
360	836	1.54	0.71	9124	14.1	0.69
380	762	1.55	0.74	6524	14.5	0.65
400	687	1.56	0.79	4649	15.3	0.62
420	614	1.56	0.80	3330	16.4	0.60
440	545	1.57	0.79	2410	17.7	0.58
460	480	1.58	0.78	1751	19.5	0.56
480	422	1.58	0.76	1296	21.7	0.55
500	370	1.59	0.75	964.4	24.5	0.53
$Mn_{1.75}Ni_{0.7}Co_{0.5-x}Cu_{0.05}Ba_xO_4$ ($x = 0.05$)						
300	2014	1.32	0.80	50,822	11.31	0.69
320	1902	1.33	0.78	38,883	11.32	0.69
340	1766	1.33	0.76	28,564	11.34	0.70
360	1619	1.34	0.74	20,458	11.35	0.71
380	1471	1.34	0.71	14,636	11.36	0.72
400	1323	1.35	0.68	10,542	11.39	0.74
420	1167	1.35	0.66	7435	11.4	0.75
440	1024	1.36	0.64	5377	11.5	0.75
460	889.3	1.36	0.63	3844	11.8	0.74
480	766.5	1.38	0.61	2729	12.2	0.74
500	665.4	1.39	0.59	2005	12.8	0.74
$Mn_{1.75}Ni_{0.7}Co_{0.5-x}Cu_{0.05}Ba_xO_4$ ($x = 0.1$)						
300	3144	1.27	0.72	107,690	10.8	0.80
320	3087	1.28	0.72	101,310	10.85	0.80
340	3031	1.29	0.72	94,669	10.89	0.80
360	2976	1.3	0.73	87,371	10.96	0.80
380	2893	1.31	0.73	77,680	10.95	0.80
400	2742	1.33	0.73	68,363	11.02	0.80
420	2607	1.34	0.73	57,407	10.97	0.80
440	2495	1.34	0.73	47,761	10.93	0.79
460	2374	1.35	0.73	38,715	10.8	0.79
480	2223	1.36	0.73	29,991	10.62	0.79
500	2069	1.36	0.73	23,178	10.43	0.78

The AC impedance spectroscopy was carried out for NTC sintered ceramics over a wide range of frequency (100 Hz to 1 MHz) to find the contribution of constituents of the microstructure, i.e., grains and grain boundary. Fig. 3 represents the Nyquist plot for respective samples measured in the frequency range of 100 Hz–1 MHz at temperature ranging from 300 °C to 500 °C. It was observed that the slopes of the curves declined and they bended towards the real Z axis with the increase in Ba content and thus the radii of curvatures were found to be

Table 4 Values of time constant (τ) determined for grain (τ_1) and grain boundary (τ_2)

Temperature (°C)	$\text{Mn}_{1.75}\text{Ni}_{0.7}\text{Co}_{0.5-x}\text{Cu}_{0.05}\text{Ba}_x\text{O}_4$ ($x = 0.0$)		$\text{Mn}_{1.75}\text{Ni}_{0.7}\text{Co}_{0.5-x}\text{Cu}_{0.05}\text{Ba}_x\text{O}_4$ ($x = 0.05$)		$\text{Mn}_{1.75}\text{Ni}_{0.7}\text{Co}_{0.5-x}\text{Cu}_{0.05}\text{Ba}_x\text{O}_4$ ($x = 0.1$)	
	τ_1 (μs)	τ_2 (μs)	τ_1 (μs)	τ_2 (μs)	τ_1 (μs)	τ_2 (μs)
300	1.59	363	2.65	575	3.99	1163
320	1.49	247	2.52	440	3.95	1099
340	1.38	173	2.34	324	3.90	1031
360	1.28	129	2.16	232	3.86	958
380	1.18	94.6	1.97	166	3.78	851
400	1.07	71.1	1.78	120	3.64	753
420	0.95	54.6	1.57	84.8	3.49	630
440	0.85	42.7	1.39	61.8	3.34	522
460	0.75	34.1	1.20	45.4	3.20	418
480	0.66	28.1	1.05	33.3	3.02	319
500	0.58	23.6	0.92	25.7	2.81	242

Time constant for both grain and grain boundary decreases with increase in temperature

decreasing with increasing temperature, which indicates the decrease in resistance of the Ba doped $\text{Mn}_{1.75}\text{Ni}_{0.7}\text{Co}_{0.5-x}\text{Cu}_{0.05}$ NTC thermistor ceramics. Generally, the presence of a single semicircular arc exhibits only one contribution, i.e., either grain interior (bulk) or grain boundary [32]. In present case, at 300 °C and higher, two semicircular arcs were observed which can be related to the presence of two different electrically active regions, i.e., grain and grain boundary. For clarification purpose, an enlarged view is presented as inset in Fig. 3a–c. Similar kind of trend was observed in all samples with increasing content of Ba as presented in Fig. 3a–c. It is also observed from Fig. 3 that the radii of curvature of the semicircular arcs tend to increase and it move away from the Z axis with increasing Ba doping indicating the increase in resistance values. ZView software (version 3.0 Scribner Associates, Inc.) was used to extract the resistance and capacitance values of grain (R_1 , C_1) and grain boundary (R_2 , C_2), respectively. For this purpose, a brick layer model was utilized to study the IS properties of desired compositions [33]. Fitting was carried out using equivalent electric circuit comprising of a two resistances (R) in series and constant phase elements (CPE) in parallel as inset shown in Fig. 3a.

In Table 3 the values of grain capacitance (C_1), grain resistance (R_1), grain boundary capacitance (C_2) and grain boundary resistance (R_2) are presented. It was observed that resistance values of both grain and grain boundary (R_1 , R_2) decreased with increase in temperature for all the samples which indicates typical NTC thermistor characteristic. It was also observed that the grain boundary resistance (R_2) is far greater in magnitude than grain resistance (R_1) and hence grain boundary resistance (R_2) is

considered as the overall impedance in NTC ceramic materials. The time constant (τ) is also calculated and presented in Table 4, for both grain and grain boundary using the relation, $\tau = RC$ where R and C are the resistance and capacitance, respectively [34, 35]. The magnitude of time constant (τ) values is in the range of 10^{-6} s that can be attributed to the conduction mechanism of hopping type [36].

The variation of imaginary part Z'' of impedance with the frequency at various temperatures from 300 °C to 500 °C for undoped and Ba doped NTC thermistors is shown in Fig. 4. It is evident from the figure that the Z'' values increased with the increase in frequency reached to maximum value, i.e., a full relaxation peak (Z''_{max}) at low frequency (<100 Hz). As temperature increased, relaxation peak (Z''_{max}) peaks shifted towards the higher frequency ranges for all the NTC ceramics samples [4, 27, 37, 38]. This appearance of temperature dependent peaks (Z''_{max}) at a characteristic frequency ($\omega_{\text{max}} = 2\pi f_{\text{max}}$) might be because of the electrical relaxation phenomena in the material, i.e., reduction in the time constant (τ) [34, 39]. These relaxation processes may be the cause of enhanced conductivity due to the presence of immobile species at lower temperature and defects at higher temperature. A clear indication of the accumulation of space charges in the materials may cause the merging of (Z''_{max}) values at extreme low and high temperature [4, 37].

Figure 5 represents the plot between the natural logarithm (ln) of both grain and grain boundary resistance (R_1 , R_2) against the reciprocal of the absolute temperature $1000/T$ (K^{-1}) with data points fitted by a linear function. It was observed that both the grain and grain boundary resistance

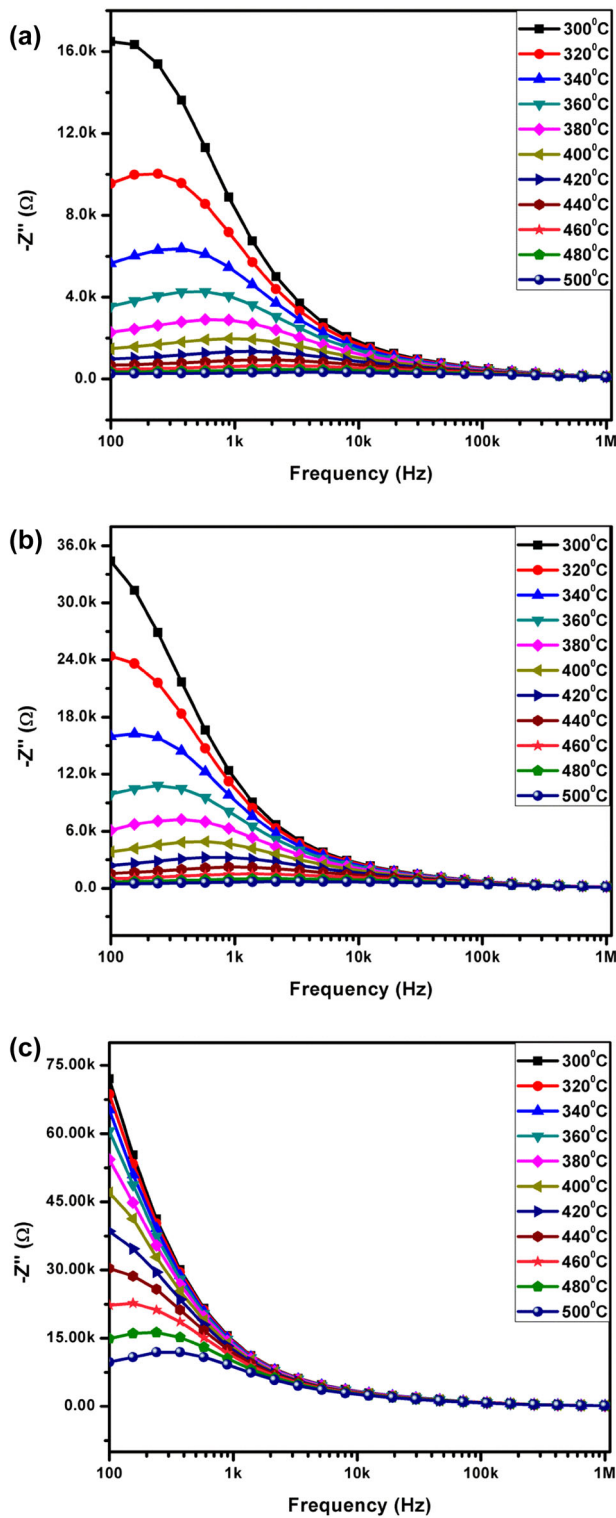


Fig. 4 Plot of imaginary part of impedance (Z'') versus frequency (100 Hz–1 MHz) for $Mn_{1.75}Ni_{0.7}Co_{0.5-x}Cu_{0.05}O_4Ba_x$, **a** $x = 0$, **b** $x = 0.05$ and **c** $x = 0.1$ NTC Thermistor ceramics

(R_1 , R_2) showed negative temperature coefficient thermistor characteristic which are in conformity with the previous work [40–42]. It can be further explained by the fact that

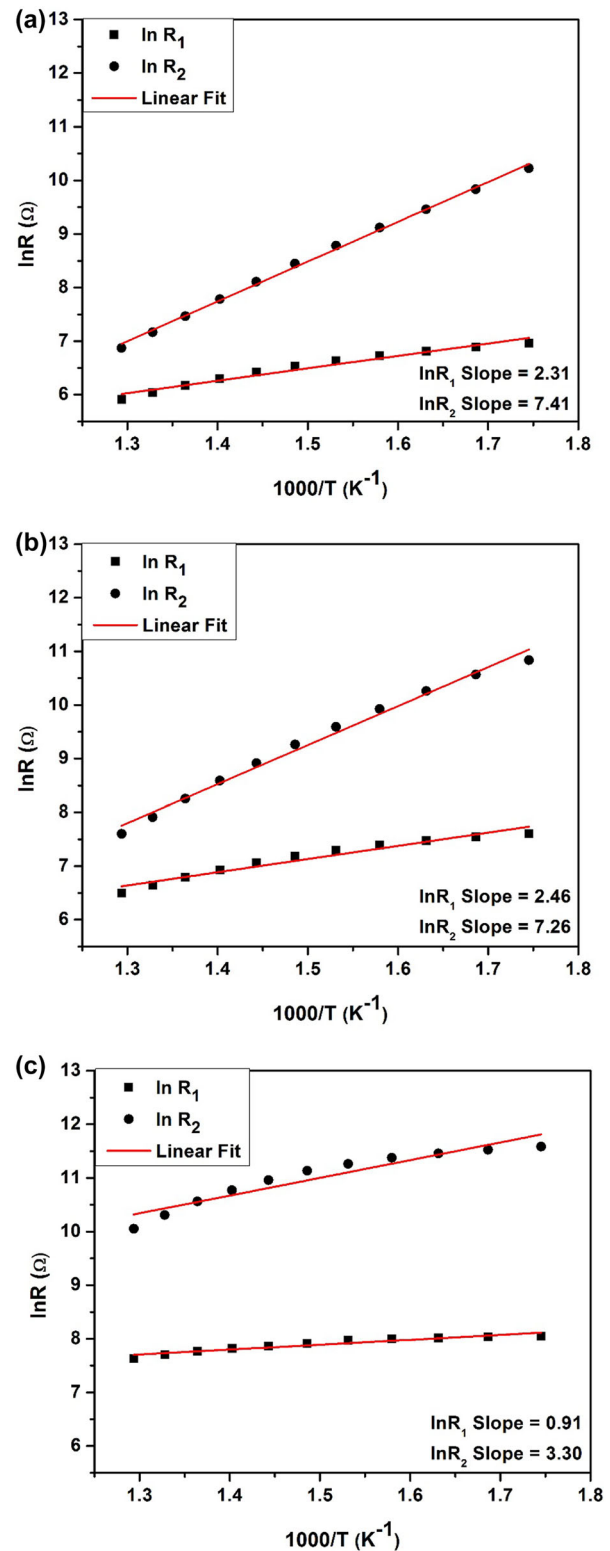


Fig. 5 Variation of logarithmic grain and grain boundary resistance ($\ln R_1$, $\ln R_2$) with reciprocal of absolute temperature for $Mn_{1.75}Ni_{0.7}Co_{0.5-x}Cu_{0.05}O_4Ba_x$, **a** $x = 0$, **b** $x = 0.05$ and **c** $x = 0.1$ NTC Thermistor ceramics

the rise in temperature may cause the increase in lattice vibration, the grain behaves as semi-conductor and the mobility of the charge carriers under acoustic wave scattering can be expressed as [4].

$$\mu_0 \propto \left[\exp\left(\frac{h\omega_1}{2\pi k_0 T}\right) - 1 \right], \quad (4)$$

where h being Planck's constant, ω_1 the vibration frequency of scattered acoustic wave, k_0 known as Boltzmann's constant and T represents absolute temperature. Equation (4) describes the mobility of charge carriers which decreases with the increase in absolute temperature. The concentration of charge carriers in grains change very little with temperature that is why the grain resistance (R_1) has very small value as compared to grain boundary resistance (R_2) [4]. As the grain boundary resistance (R_2) also decreases with temperature and is far greater in magnitude than grain resistance (R_1), so it contributes to the overall resistance of the material which thus represents the NTC thermistor characteristics. It is also concluded that the NTC thermistor characteristics of Ba doped $\text{Mn}_{1.75}\text{Ni}_{0.7}\text{Co}_{0.5-x}\text{Cu}_{0.05}$ mainly relies on the grain boundary resistance (R_2).

4 Conclusion

Polycrystalline $\text{Mn}_{1.75}\text{Ni}_{0.7}\text{Co}_{0.5-x}\text{Cu}_{0.05}\text{Ba}_x\text{O}_4$ ($x = 0, 0.05$ and 0.1) based NTC ceramics were successfully synthesized by solid state reaction method. XRD studies revealed cubic spinel structure without showing any secondary phase. SEM analysis showed a dense microstructure with slight increase in grain size as the concentration of Ba dopant increased. Overall impedance was found to be composed of two contributions, i.e., grain and grain boundary resistance. However, grain boundary resistance was several times greater than the resistance of grains implying that the NTC characteristic of doped samples is mainly dependent on grain boundaries. It was evident that in the temperature range of $300\text{--}500$ °C, both the grain and grain boundary resistance linearly decreased showing an excellent NTC thermistor behavior. These results can be quite useful in designing the optimum microstructure for specific applications.

References

- R. Jadhav, S. Mathad, V. Puri, Studies on the properties of $\text{Ni}_{0.6}\text{Cu}_{0.4}\text{Mn}_2\text{O}_4$ NTC ceramic due to Fe doping. *Ceram. Int.* **38**(6), 5181–5188 (2012)
- J.M. Varghese, A. Seema, K.R. Dayas, Microstructural, electrical and reliability aspects of chromium doped Ni–Mn–Fe–O NTC thermistor materials. *Mater. Sci. Eng., B* **149**(1), 47–52 (2008)
- M.N. Muralidharan et al., Optimization of process parameters for the production of Ni–Mn–Co–Fe based NTC chip thermistors through tape casting route. *J. Alloy. Compd.* **509**(38), 9363–9371 (2011)
- J. Xia et al., Sintering temperature and impedance analysis of $\text{Mn}_{0.9}\text{Co}_{1.2}\text{Ni}_{0.27}\text{Mg}_{0.15}\text{Al}_{0.03}\text{Fe}_{0.45}\text{O}_4$ NTC ceramic prepared by W/O microemulsion method. *J. Alloy. Compd.* **617**, 228–234 (2014)
- K. Park et al., Improvement in the electrical stability of Mn–Ni–Co–O NTC thermistors by substituting Cr_2O_3 for Co_3O_4 . *J. Alloy. Compd.* **437**(1), 211–214 (2007)
- K. Park et al., Structural and electrical properties of MgO-doped $\text{Mn}_{1.4}\text{Ni}_{1.2}\text{Co}_{0.4-x}\text{Mg}_x\text{O}_4$ ($0 \leq x \leq 0.25$) NTC thermistors. *J. Eur. Ceram. Soc.* **27**(4), 2009–2016 (2007)
- W. Wang et al., Synthesis of nanocrystalline $\text{Ni}_1\text{Co}_{0.2}\text{Mn}_{1.8}\text{O}_4$ powders for NTC thermistor by a gel auto-combustion process. *Ceram. Int.* **33**(3), 459–462 (2007)
- M. Hosseini, The effect of cation composition on the electrical properties and aging of Mn–Co–Ni thermistors. *Ceram. Int.* **26**(3), 245–249 (2000)
- K. Park, I. Han, Effect of Cr_2O_3 addition on the microstructure and electrical properties of Mn–Ni–Co oxides NTC thermistors. *J. Electroceram.* **17**(2–4), 1069–1073 (2006)
- J.M. Varghese, A. Seema, K. Dayas, Microstructural, electrical and reliability aspects of chromium doped Ni–Mn–Fe–O NTC thermistor materials. *Mater. Sci. Eng. B* **149**(1), 47–52 (2008)
- R.C. Buchanan, *Ceramic materials for electronics: processing, properties, and applications* (Marcel Dekker, NY, USA, 1986)
- R. Jadhav, S. Mathad, V. Puri, Studies on the properties of $\text{Ni}_{0.6}\text{Cu}_{0.4}\text{Mn}_2\text{O}_4$ NTC ceramic due to Fe doping. *Ceram. Int.* **38**(6), 5181–5188 (2012)
- M. Muralidharan et al., Effect of Cu and Fe addition on electrical properties of Ni–Mn–Co–O NTC thermistor compositions. *Ceram. Int.* **38**(8), 6481–6486 (2012)
- H. Zhang, A. Chang, C. Peng, Preparation and characterization of Fe^{3+} -doped $\text{Ni}_{0.9}\text{Co}_{0.8}\text{Mn}_{1.3-x}\text{Fe}_x\text{O}_4$ ($0 \leq x \leq 0.7$) negative temperature coefficient ceramic materials. *Microelectron. Eng.* **88**(9), 2934–2940 (2011)
- J. Xia et al., Synthesis and properties of $\text{Mn}_{1.05-y}\text{Co}_{1.95-x-z-w}\text{Ni}_x\text{Mg}_y\text{Al}_z\text{Fe}_w\text{O}_4$ NTC ceramic by co-precipitation method. *J. Alloy. Compd.* **646**, 249–256 (2015)
- K. Park, D. Bang, Electrical properties of Ni–Mn–Co–(Fe) oxide thick-film NTC thermistors prepared by screen printing. *J. Mater. Sci.: Mater. Electron.* **14**(2), 81–87 (2003)
- K. Park et al., Influence of the composition and the sintering temperature on the electrical resistivities of Ni–Mn–Co–(Fe) oxide NTC thermistors. *J. Korean Phys Soc* **41**(2), 251–256 (2002)
- K. Park, J. Lee, The effect of ZnO content and sintering temperature on the electrical properties of Cu-containing $\text{Mn}_{1.95-x}\text{Ni}_{0.45}\text{Co}_{0.15}\text{Cu}_{0.45}\text{Zn}_x\text{O}_4$ ($0 \leq x \leq 0.3$) NTC thermistors. *J. Alloy. Compd.* **475**(1), 513–517 (2009)
- M. Muralidharan et al., Optimization of process parameters for the production of Ni–Mn–Co–Fe based NTC chip thermistors through tape casting route. *J. Alloy. Compd.* **509**(38), 9363–9371 (2011)
- K. Park et al., The effect of Zn on the microstructure and electrical properties of $\text{Mn}_{1.17-x}\text{Ni}_{0.93}\text{Co}_{0.9}\text{Zn}_x\text{O}_4$ ($0 \leq x \leq 0.075$) NTC thermistors. *J. Alloy. Compd.* **467**(1), 310–316 (2009)
- R. Jadhav, S. Mathad, V. Puri, Studies on the properties of $\text{Ni}_{0.6}\text{Cu}_{0.4}\text{Mn}_2\text{O}_4$ NTC ceramic due to Fe doping. *Ceram. Int.* **38**(6), 5181–5188 (2012)
- C. Yuan et al., Electrical properties of $\text{Sr}_x\text{Ba}_{1-x}\text{Fe}_{0.6}\text{Sn}_{0.4}\text{O}_{3-x}$ NTC thermistors. *Bull. Mater. Sci.* **35**(3), 425–431 (2012)
- R.D. Shannon, Revised effective ionic radii and systematic studies of interatomic distances in halides and chalcogenides. *Acta Crystallogr Sect A* **32**(5), 751–767 (1976)

24. D.C. Sinclair, A.R. West, Impedance and modulus spectroscopy of semiconducting BaTiO₃ showing positive temperature coefficient of resistance. *J. Appl. Phys.* **66**(8), 3850–3856 (1989)
25. J.R. Macdonald, W.B. Johnson, Fundamentals of Impedance Spectroscopy, in *Impedance Spectroscopy: Theory, Experiment, and Applications*, edn. 2. (Wiley, NJ, USA, 2005), pp. 1–26
26. M.A. Rafiq, M.N. Rafiq, K.V. Saravanan, Dielectric and impedance spectroscopic studies of lead-free barium-calcium-zirconium-titanium oxide ceramics. *Ceram. Int.* **41**(9), 11436–11444 (2015)
27. S. Song, Z. Ling, F. Placido, Impedance analysis of MnCoCuO NTC ceramic. *Mater. Res. Bull.* **40**(7), 1081–1093 (2005)
28. M.A. Rafiq et al., Impedance analysis and conduction mechanisms of lead free potassium sodium niobate (KNN) single crystals and polycrystals: a comparison study. *Cryst. Growth Des.* **15**(3), 1289–1294 (2015)
29. H. Zhang, A. Chang, C. Peng, Preparation and characterization of Fe³⁺-doped Ni_{0.9}Co_{0.8}Mn_{1.3-x}Fe_xO₄ (0 ≤ x ≤ 0.7) negative temperature coefficient ceramic materials. *Microelectron. Eng.* **88**(9), 2934–2940 (2011)
30. K. Park et al., Structural and electrical properties of MgO-doped Mn_{1.4}Ni_{1.2}Co_{0.4-x}Mg_xO₄ (0 ≤ x ≤ 0.25) NTC thermistors. *J. Eur. Ceram. Soc.* **27**(4), 2009–2016 (2007)
31. S. Jagtap et al., Study of microstructure, impedance and dc electrical properties of RuO₂-spinel based screen printed 'green'NTC thermistor. *Curr. Appl. Phys.* **10**(4), 1156–1163 (2010)
32. N. Hirose, A.R. West, Impedance spectroscopy of undoped BaTiO₃ ceramics. *J. Am. Ceram. Soc.* **79**(6), 1633–1641 (1996)
33. J. Fleig, J. Maier, The influence of laterally inhomogeneous contacts on the impedance of solid materials: a three-dimensional finite-element study. *J. Electroceram.* **1**(1), 73–89 (1997)
34. A. Kamal et al., Structural and impedance spectroscopic studies of CuO-doped (K_{0.5}Na_{0.5}Nb_{0.995}Mn_{0.005}O₃) lead-free piezoelectric ceramics. *Appl. Phys. A* **122**(12), 1037 (2016)
35. Q.K. Muhammad et al., Structural, dielectric, and impedance study of ZnO-doped barium zirconium titanate (BZT) ceramics. *J. Mater. Sci.* **51**(22), 10048–10058 (2016)
36. K.C. Kao, *Dielectric phenomena in solids* (Academic Press, London, 2004)
37. R. Sagar, R. Raibagkar, Complex impedance and modulus studies of cerium doped barium zirconium titanate solid solution. *J. Alloy. Compd.* **549**, 206–212 (2013)
38. C. Suman, K. Prasad, R. Choudhary, Impedance analysis of Pb₂Sb₃LaTi₅O₁₈ ceramic. *Mater. Chem. Phys.* **97**(2), 425–430 (2006)
39. A.K. Jonscher, The universal dielectric response. *Nature* **267**, 673–679 (1977)
40. J. Xia et al., Sintering temperature and impedance analysis of Mn_{0.9}Co_{1.2}Ni_{0.27}Mg_{0.15}Al_{0.03}Fe_{0.45}O₄ NTC ceramic prepared by W/O microemulsion method. *J. Alloy. Compd.* **617**, 228–234 (2014)
41. K. Park et al., Structural and electrical properties of MgO-doped Mn_{1.4}Ni_{1.2}Co_{0.4-x}Mg_xO₄ (0 ≤ x ≤ 0.25) NTC thermistors. *J. Eur. Ceram. Soc.* **27**(4), 2009–2016 (2007)
42. J. Xia et al., Synthesis and properties of Mn_{1.05-y}Co_{1.95-x-z-w}Ni_xMg_yAl_zFe_wO₄ NTC ceramic by co-precipitation method. *J. Alloy. Compd.* **646**, 249–256 (2015)